

Super-transient scaling in time-delay autonomous Boolean network motifs

Otti D'Huys¹, Johannes Lohmann, Nicholas D. Haynes, and Daniel J. Gauthier

Citation: *Chaos* **26**, 094810 (2016); doi: 10.1063/1.4954274

View online: <http://dx.doi.org/10.1063/1.4954274>

View Table of Contents: <http://aip.scitation.org/toc/cha/26/9>

Published by the [American Institute of Physics](#)

Welcome to a

Smarter Search 

PHYSICS
TODAY

with the redesigned
Physics Today Buyer's Guide

Find the tools you're looking for today!

Super-transient scaling in time-delay autonomous Boolean network motifs

Otti D’Huys,^{1,a)} Johannes Lohmann,^{1,2} Nicholas D. Haynes,¹ and Daniel J. Gauthier^{1,3}

¹Department of Physics, Duke University, Durham, North Carolina 27708, USA

²Institut für Theoretische Physik, Technische Universität Berlin, Hardenbergstraße 36, 10623 Berlin, Germany

³Department of Physics, The Ohio State University, Columbus, Ohio 43210, USA

(Received 25 March 2016; accepted 26 May 2016; published online 7 July 2016)

Autonomous Boolean networks are commonly used to model the dynamics of gene regulatory networks and allow for the prediction of stable dynamical attractors. However, most models do not account for time delays along the network links and noise, which are crucial features of real biological systems. Concentrating on two paradigmatic motifs, the toggle switch and the repressilator, we develop an experimental testbed that explicitly includes both inter-node time delays and noise using digital logic elements on field-programmable gate arrays. We observe transients that last millions to billions of characteristic time scales and scale exponentially with the amount of time delays between nodes, a phenomenon known as super-transient scaling. We develop a hybrid model that includes time delays along network links and allows for stochastic variation in the delays. Using this model, we explain the observed super-transient scaling of both motifs and recreate the experimentally measured transient distributions. *Published by AIP Publishing.*

[<http://dx.doi.org/10.1063/1.4954274>]

Gene regulatory networks control many essential biological functions, including cell differentiation and metabolism, and autonomous Boolean networks (ABNs) are a common model to describe their dynamical behavior. Most existing work, however, does not account for interaction delays and stochastic noise that is present in the underlying biological systems. To address these shortcomings, we use high-speed digital electronics to construct physical ABNs with inter-node time delays. Our experimental system allows us to create networks with arbitrary topologies and controllable delays between nodes and includes a host of non-ideal effects that may also play a role in a biological context. We study two small network motifs and find that, although the predicted stable states of these systems are eventually reached, the time to reach these attractors scales exponentially with the time delay. This phenomenon is known as super-transient scaling, and the durations of these experimentally observed super-transients raise the question of whether transients might have relevance in a biological context.

I. INTRODUCTION

The dynamical behavior of gene regulatory networks is commonly described by a set of piecewise linear differential equations known as autonomous Boolean networks (ABNs) or the Glass model.^{1–6} The process of gene regulation involves individual genes, coding for a protein, called the gene product. This gene product, also called a transcription factor, regulates in turn the transcription rate of other genes. In the Glass model, the genetic activity is represented by a Boolean variable, obtained by thresholding the concentration of its transcription factor: a gene is either expressed (“on”),

meaning that it is transcribed and its gene product is being produced, or not expressed (“off”). The associated gene product concentration evolves continuously depending on its response time and the (Boolean) transcription rate.

The attractor structure of ABNs has been used to explain different patterns of genetic activity and could thus describe phenomena such as stem cell differentiation, cell evolution, and determine the immune response of a cell.^{7–9} For small-scale ABNs, the complete attractor structure can be determined analytically, and the dynamical evolution of the network’s state can be visualized as a walk along a “Boolean hypercube,”^{5,10,11} as shown in Fig. 1. In this visualization, the 2^N possible states of an N -node network are represented as the 2^N corners of a N -dimensional hypercube, and allowed state transitions are represented as the directed edges of this hypercube.

The biochemical processes underlying gene regulation involve many steps,^{12,13} however, and these intermediate interactions can give rise to time delays in the response of a gene to changing environmental conditions.^{14–16} Moreover, this delay may vary stochastically, given that small quantities of genes involved in the reaction can lead to pronounced effects.^{17,18} In previous work on ABNs that does not include time delays, transients are short lived and the stable attractor is reached quickly. We demonstrate, however, that the explicit inclusion of interaction delays generates super-transients.

Super-transients in delay systems, which scale exponentially with the time delay, have been theoretically studied in a context of bistable delayed feedback systems, which appear frequently in optics and biology^{19,20} and have been termed “metastable patterns”. In a context of two delay-coupled Hopfield neurons, the phenomenon has been named “delay induced transient oscillations.”²¹ Mathematically similar to gene regulatory circuits, these are all bistable switchlike systems, and the approximation as a piecewise linear systems proves useful as well. Our work thus provides experimental

^{a)}Electronic mail: otti.dhuys@phy.duke.edu

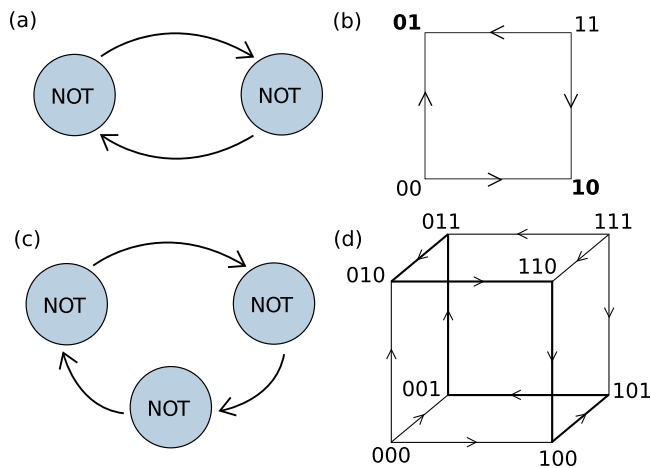


FIG. 1. Cartoon topology and Boolean hypercube state space visualization of the toggle switch [(a) and (b)] and repressilator [(c) and (d)]. Transitions allowed by network topology are indicated with arrows, and stable states are bolded. In the case of the toggle switch, the states $\{0, 1\}$ and $\{1, 0\}$ are stable fixed points, and in the case of the repressilator, the path $\{0, 1, 0\} \rightarrow \{1, 1, 0\} \rightarrow \{1, 0, 0\} \rightarrow \{0, 0, 1\} \rightarrow \{0, 1, 1\}$ is a stable limit cycle.

evidence for this behavior, and extends the past research to larger networks and stochastic delays.

Our results are not only relevant in a context of ABNs. Although dynamical systems are often analyzed in terms of their stable attractors, supertransients might render the eventual attractor irrelevant.^{22,23} We show that link delays—which appear, but are not always taken into account in many complex networks, such as neuronal networks and gene regulatory networks can give rise to transients that might be so long, that, in order to understand or control the dynamics, analyzing the structure of the stable attractors is not sufficient.

In this work, we consider two paradigmatic network motifs—the toggle switch and the repressilator, illustrated in Fig. 1. The toggle switch is a bistable motif of two mutually repressing genes, the repressilator is a unidirectional ring of three genes that repress one another, and shows stable out-of-phase oscillations. Both motifs have been synthesized in biological systems.^{24,25} We study the super-transient dynamics of these network motifs with delays both experimentally and theoretically. First, as described in Sec. II, we construct experimental autonomous Boolean networks using fast digital electronics. We represent repressing genes as inverter gates in a digital circuit and explicitly include delays between the nodes. We find that the toggle switch and repressilator circuits do indeed reach the stable behavior predicted by the Glass model, but that the unstable transient dynamics leading to the attractor can be extremely long-lived. These long transients can last for millions or even billions of characteristic time scales and their duration approximates an exponential scaling with the delay. The sheer magnitude of the super-transients may render the stable behavior of these systems irrelevant in some circumstances.^{22,23}

We then introduce an analytical model based on the Glass model that includes interaction delays in Sec. III. We derive explicit transient times for the toggle switch and repressilator and demonstrate that the model reproduces metastability that is observed experimentally. Moreover, we

allow interaction delays to vary stochastically and show how noise affects the metastability and explains the experimentally observed probability distributions.

II. EXPERIMENTAL SYSTEM AND RESULTS

Field-programmable gate arrays (FPGAs) are a type of programmable integrated circuit that can be used to synthesize large, experimental complex networks with arbitrary topologies, asynchronous (i.e., unclocked) update rules, and time-delay links.²⁶ Nodes of these experimental autonomous Boolean networks are built from asynchronous logic elements on the FPGA, which can be configured to perform arbitrary Boolean functions. By wiring a specific number of “delay elements” consisting of pairs of inverter gates in series, the finite rise and fall times of the logic elements can be exploited to create links with a specific amount of time delay.^{26,27}

We use an Altera Cyclone IV FPGA to construct two paradigmatic network motifs—the toggle switch and the repressilator, which consist of two and three unidirectionally coupled inverters, respectively—and vary the amount of delay between each of the nodes to study the transient evolution of these systems to their stable states. The average delay of a single delay element on the Cyclone IV is experimentally measured to be 520 ps, though heterogeneity between logic elements due to chip architecture and manufacturing imperfections causes the possible delay to vary between 250 and 750 ps. Here, we consider only the case where the number of delay elements, denoted $n = (n_1, n_2, \dots, n_N)$, with N being the number of links, is the same, i.e., $n_1 = n_2 = \dots = n_N$.

We study the scaling of average transient durations by implementing a given network topology on the FPGA and increasing the time delay between nodes. Initial conditions of the networks are specified by holding each of the nodes in either the 0 or 1 state for a period of 60 ms. The networks begin their dynamical evolution when the nodes are released simultaneously (to within 100 ps) from their initial conditions by a control signal from a clocked register. At this point, the dynamical state of each node evolves asynchronously with its inputs until a stable state of the network is reached. A 50 MHz counter implemented on the FPGA records the time elapsed from when the network is released from its initial conditions to when the stable behavior is detected with a precision of 20 ns. For each n , approximately 3×10^4 transients are recorded to produce histograms that estimate the probability density function of the transient durations.

Toggle switch—The dynamical evolution of the toggle switch with no delay ($n=0$) is illustrated in Fig. 1(b). It is seen that the states $(0, 1)$ and $(1, 0)$ are stable fixed points. If the network is initialized in any other state, it quickly evolves to one of these two fixed points and remains there for all time.¹

An example of the evolution of an experimentally-realized toggle switch with time delays is shown in Fig. 2. A toggle switch with time delays of $n=(2, 2)$ delay elements along its links is initialized with both nodes in the 0 state. Immediately after being released, the network displays in-

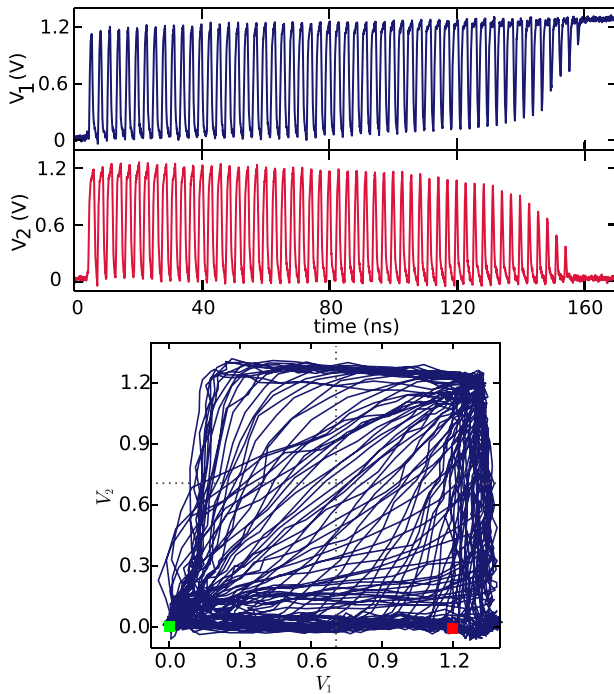


FIG. 2. (a) Time series of a network of a toggle switch with $n=2$ delay elements (approximately 1.2 ns) between each node initialized with both nodes in the 0 state. The oscillatory transient collapses to the (1, 0) state after approximately 150 ns. (b) Phase diagram of the same time series. The green square indicates the initial conditions in the (0, 0) state, and the red square indicates the fixed point of (1, 0) reached by the network.

phase oscillations. Over time, however, heterogeneities in the network cause a shortening of the pulses generated by each node. When the pulses become shorter than the response time of the nodes (approximately 410 ps), the pulses are rejected outright and the network collapses into a stable state.

We find that the mean transient duration T_m of toggle switches tends to increase non-monotonically with the amount of time delay between the nodes, as shown in Fig. 3. The exponential trend is however clear. For transients of moderate length (i.e., hundreds to thousands of oscillations), the distributions of durations are short-tailed. As the time delays along the links are increased above $\tau \approx 2$ ns, however,

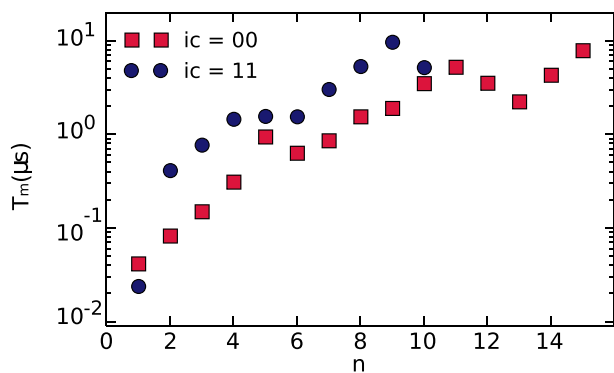


FIG. 3. Mean transient duration T_m for the toggle switch increase non-monotonically as the number of delay elements between the nodes is increased for initial conditions (ic) (0, 0) (red squares) and (1, 1) (blue dots). Standard deviations are smaller than the width of the markers and are omitted.

for some experimental realizations the tail of the distributions becomes dramatically longer and resembles a power law. Moreover, the mean transient duration T_m is different for the two initial conditions that we used. Typical probability mass functions of the transient times in the short-tail (long-tail) regime are shown in Fig. 4(a) (Fig. 4(b)). In addition, some choices of delays give rise to bistability, in which networks initialized with nominally the same initial conditions eventually collapse to either of two co-existing stable attractors, (0, 1) or (1, 0).

The super-transients with broad distributions in toggle switches only occur for specific values of delays, however. We relate this phenomenon, as well as the nonmonotonic scaling of the transient length, and the difference between the two initial conditions that we used, to the high sensitivity of the circuit to small differences between the logical gates, which cause a heterogeneity between the link delays. Moreover, the gates can show a difference in response time between the upward transition and the downward transition.^{26,28} These rise/fall asymmetries are as well specific for each node, and combine to a rise/fall asymmetry over the whole delay line. The effect is theoretically modeled in Section III D.

Repressilator—We perform similar experiments for the repressilator. The allowed dynamical transitions of a repressilator with no delay are shown in Fig. 1(d). For this network, it can be seen that the limit cycle $\{0, 1, 0\} \rightarrow \{1, 1, 0\} \rightarrow \{1, 0, 0\} \rightarrow \{1, 0, 1\} \rightarrow \{0, 0, 1\} \rightarrow \{0, 1, 1\}$ is stable. A network with initial conditions not on this limit cycle quickly evolves to this stable behavior.¹

The mean transient length T_m of the repressilator is shown in Fig. 5. Also here we observe an exponential trend, which is deteriorated by a high sensitivity to the specific setup (data for $n=6$ and $n=7$ do not follow this trend). Just like for the toggle switch, we find that transients for a repressilator with short delays are moderate in duration and short-tailed, but a regime of super-transients is observed as link

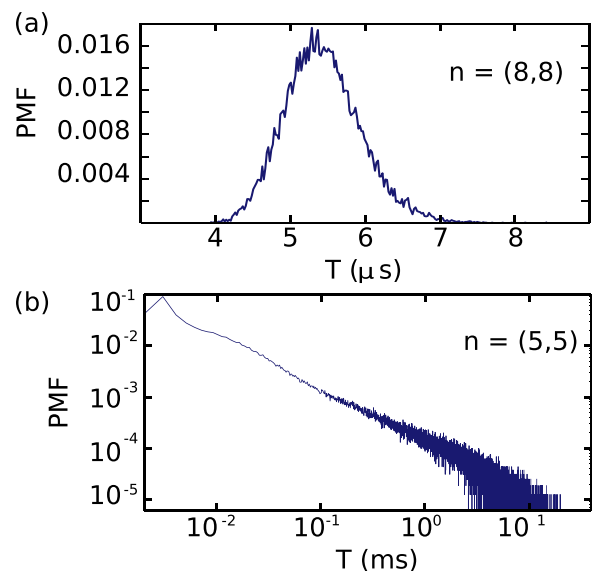


FIG. 4. Probability mass functions of toggle switch transients (a) with short-tailed durations for $n=(8, 8)$ delay elements (approximately 4.8 ns) between the nodes and (b) with long-tailed (power law) durations for $n=(5, 5)$ delay elements (approximately 3 ns) between the nodes.

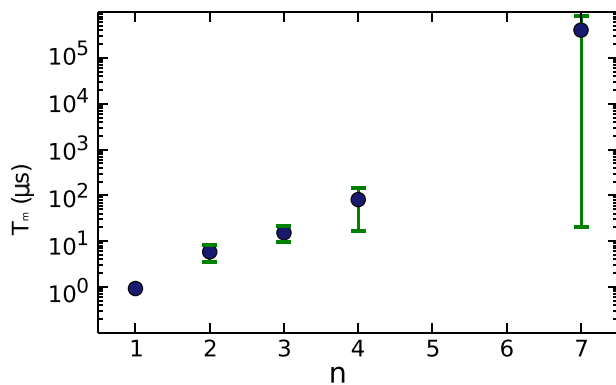


FIG. 5. Mean transient durations T_m for the repressilator increase exponentially (and monotonically) as the number of delay elements between the nodes is increased. The transition from short-tailed to long-tailed distributions can be seen in the growth of the vertical bars, which indicate the standard deviation of the distribution.

delays are increased above $\tau \approx 2$ ns. The observed supertransients for the repressilator are however much longer on average than for the toggle switch, lasting as long as seconds or even minutes (corresponding to billions of oscillations cycles). As shown in Fig. 6(b), the tails are distributed exponentially for a repressilator, as opposed to the power law tails observed for the toggle switch. Unlike for the toggle switch, repressilator supertransients are found for every network with delay times larger than $\tau \approx 2$ ns.

This difference between toggle switch and repressilator can be explained by a symmetry argument: In rings with an odd numbers of inverter gates, such as the repressilator, upward transitions become downward transitions on successive passes around the ring, thus correcting the rise/fall asymmetry. This correction does not occur, however, for rings with even numbers of logic elements, resulting in pulses that are broadened or narrowed on successive passes through the ring. The rise/fall asymmetry therefore biases

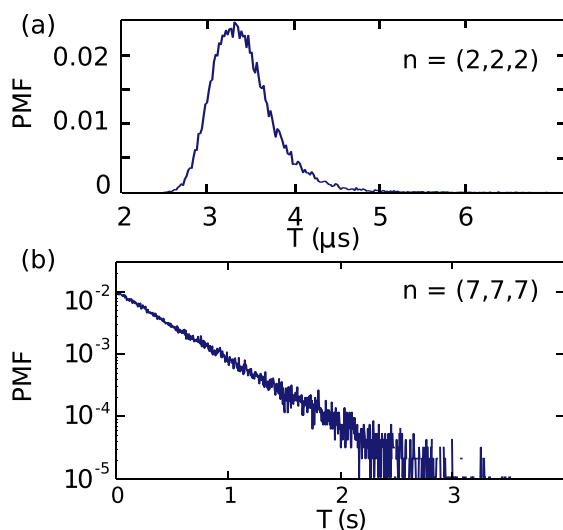


FIG. 6. Probability mass functions of the transient durations for repressilators with (a) $n = (2, 2, 2)$ delay elements (approximately 1.2 ns) and (b) $n = (7, 7, 7)$ delay elements (approximately 4.2 ns). The repressilator consistently produces short-tailed transient distributions for short delay and long-tailed transient distributions for long delay.

the toggle switch toward one of the stable states over time, decreasing the likelihood of extremely long-lived transients.

III. ANALYTIC MODEL

We use a piecewise linear model with delay to explain our experimental results. First, we explicitly derive the duration of transient times for a symmetric toggle switch and repressilator, and we recover an exponential dependence of the transient duration on the delay time. Next, we explain how, in the toggle switch, heterogeneities in the time delays and asymmetries in rise and fall times of the different gates, implemented as asymmetric thresholds, affect the duration of the transient, and how their combined effect can lead to a non-monotonic behavior of the transient duration with the delay, whereas, in a repressilator, the effect of threshold asymmetries is shown to be much smaller. Finally, we explicitly implement stochasticity in the time delays and explain the experimentally observed transient time distributions.

A. Piecewise linear modeling of a ring of inverters

Following Edwards *et al.*,¹⁶ we model a ring of N inverters as

$$\dot{x}_i(t) = -x_i(t) + F(x_{i+1}(t - \tau_i)), \quad (1)$$

with $i = 1 \dots N$ and $N + 1 \equiv 1$. The function $F(x)$ represents an inverter gate, which asynchronously thresholds and inverts its input. We chose here the “on” state as $x = 1$ and the “off” state as $x = -1$ for the sake of symmetry, i.e.,

$$F(x) = \begin{cases} 1 & \text{if } x < 0 \\ -1 & \text{if } x \geq 0. \end{cases} \quad (2)$$

Inspired by the Glass model,¹ this model (Eq. (1)) takes into account an internal response time of the signal. As the input signal $F(x)$ switches, the output follows exponentially. This response time, which is measured experimentally to be approximately 410 ps, is normalized to unity in our model. In contrast to the Glass model, we also include a delay time τ_i of each link.

Since the modeling equations are piecewise linear, it is possible to treat the system analytically. The system allows for almost synchronous in-phase oscillations. The inverters are slightly time-shifted²⁹ and exhibit square-wave oscillations with a period $P = 2\tau + 2\ln(2 - e^{-\tau})$, with τ being the average delay in the ring. The motion is then described as

$$\begin{aligned} x(t) &= -1 + (2 - e^{-\tau})e^{-t-nP} \\ &\quad \text{for } nP \leq t < nP + P/2 \\ x(t) &= -x(t - P/2) \\ &\quad \text{for } nP + P/2 \leq t < (n+1)P. \end{aligned} \quad (3)$$

This solution exists in a ring of any number of elements, but it is unstable if there is more than one inverter.

B. Transient duration in the toggle switch

We calculate explicitly the transient time to reach the stable state for a toggle switch with heterogeneous delays, starting from initial conditions $x_1(t \leq 0) = x_2(t \leq 0) = 1$. A

difference in link delays is mathematically equivalent to a difference in initial conditions, as long as the number of edges is the same: one can transform²⁹ a system with the same delays $\tau_1 = \tau_2 = \tau$ and different initial conditions $x_1(-\tau < t \leq -\tau + \Delta) = -1$, $x_1(-\tau + \Delta < t \leq 0) = 1$ and $x_2(t \leq 0) = 1$, into a system with the same initial conditions $x_1(t \leq 0) = x_2(t \leq 0) = 1$ and heterogeneous delays $\tau_{1,2} = \tau \mp \Delta$. The heterogeneity in our model $\tau_2 - \tau_1$ thus results from the combination of different link delays and differences in timing at the initialization of the nodes. We reformulate the dynamics of toggle switch as a map.¹⁶ Our method is based on the approach of Pakdaman *et al.*,²¹ and extends and refines their results, to include multiple inverters, asymmetry and stochastic delays.

The electronic toggle switch is modeled as

$$\begin{aligned} \dot{x}_1 &= -x_1 + F(x_2(t - \tau_1)) \\ \dot{x}_2 &= -x_2 + F(x_1(t - \tau_2)). \end{aligned} \tag{4}$$

Initializing the inverter gates as $x_1(t) = x_2(t) = 1$ for $t \leq 0$, we find that both inverters evolve exponentially towards the ‘‘off’’ state as the system is released

$$x_1(t) = x_2(t) = -1 + 2e^{-t}. \tag{5}$$

At $t_0 = \ln(2)$ the inverters cross the threshold $x = 0$. Consequently, at $t_{1,1} = t_0 + \tau_1$, $x_1(t)$ changes direction. The other inverter $x_2(t)$ switches direction at $t_{1,2} = t_0 + \tau_2$. We define a_1 and b_1 as the respective distances of the inverters from the steady states $x = \pm 1$

$$\begin{aligned} a_1 &= |1 + x_1(t_{1,1})| = e^{-\tau_1} \\ b_1 &= |1 + x_2(t_{1,2})| = e^{-\tau_2}. \end{aligned} \tag{6}$$

For $\tau_1 < \tau_2$, we find $b_1 < a_1$, meaning that the second inverter comes closer to the steady state than the first one. In the next delay interval $t > t_{1,i}$, the inverters evolve towards the ‘‘on’’ state again. Their dynamics are given by

$$\begin{aligned} x_1(t) &= 1 - (2 - a_1)e^{-(t-t_{1,1})} \\ x_2(t) &= 1 - (2 - b_1)e^{-(t-t_{1,2})}. \end{aligned} \tag{7}$$

The difference in amplitude between the voltages causes an additional difference in timing between the edges. We find for the next switching points

$$\begin{aligned} t_{2,1} &= t_{1,2} + \ln(2 - b_1) + \tau_1 \\ t_{2,2} &= t_{1,1} + \ln(2 - a_1) + \tau_2, \end{aligned} \tag{8}$$

such that the plateau lengths are given by

$$\begin{aligned} \Delta t_1 &= t_{2,1} - t_{1,1} = \tau_2 + \ln(2 - b_1) \\ \Delta t_2 &= t_{2,2} - t_{1,2} = \tau_1 + \ln(2 - a_1). \end{aligned} \tag{9}$$

As each inverter shows asymmetric square waves with approximate plateau lengths $\tau_1 + \ln 2$ and $\tau_2 + \ln 2$, we define a_k and b_k as the distances from ± 1 for the short and the long plateaus, respectively. We thus follow a plateau, rather than an inverter. The next distances a_2 and b_2 are given by

$$\begin{aligned} a_2 &= |1 - x_2(t_{2,2})| = (2 - b_1)e^{-\Delta t_2} = \frac{2 - b_1}{2 - a_1} e^{-\tau_1} \\ b_2 &= |1 - x_1(t_{2,1})| = (2 - a_1)e^{-\Delta t_1} = \frac{2 - a_1}{2 - b_1} e^{-\tau_2}. \end{aligned} \tag{10}$$

Following this method, we can predict the minimal and maximal voltages (and plateau lengths) over the next delay intervals. This leads to a map

$$\begin{aligned} a_{k+1} &= \frac{2 - b_k}{2 - a_k} a_k \\ b_{k+1} &= \frac{2 - a_k}{2 - b_k} b_k. \end{aligned} \tag{11}$$

Using $a_1 = e^{-\tau_1}$ and $b_1 = e^{-\tau_2}$, we find $a_k b_k = e^{-(\tau_1 + \tau_2)}$. At each transition, the series b_k converges to zero while the series a_k diverges, i.e., the difference between the amplitudes of the oscillators increases. When $a_K \geq 1$, we find $x_1(t_{1,K}) = a_K - 1 > 0$ (or $x_2(t_{2,K}) = 1 - a_K < 0$) at the onset of an upward (downward) transition. As one of the inverters does not cross the threshold, the pulse is not being transmitted and the steady state is reached.

The map (11) can be explicitly written as

$$a_k = e^{-\tau_1} \frac{\left((2 + e^{-\tau})^k + (2 - e^{-\tau})^k \right) - e^{\frac{\tau_1 - \tau_2}{2}} \left((2 + e^{-\tau})^k - (2 - e^{-\tau})^k \right)}{\left((2 + e^{-\tau})^k + (2 - e^{-\tau})^k \right) - e^{\frac{\tau_2 - \tau_1}{2}} \left((2 + e^{-\tau})^k - (2 - e^{-\tau})^k \right)}, \tag{12}$$

with $\tau = \frac{1}{2}(\tau_1 + \tau_2)$. The transient length is given by $T = K(\tau + \ln(2 - e^{-\tau}))$, where K is determined by the condition $a_K > 1$, multiplied by the mean plateau length. In the long delay limit $e^{-\tau} \rightarrow 0$, we can approximate

$$\begin{aligned} 0 &\approx \frac{e^{-\tau_1}}{a_K} = \frac{e^{-\tau_1}}{\left((2 + e^{-\tau})^K + (2 - e^{-\tau})^K \right)} \\ &\quad - e^{\frac{\tau_2 - \tau_1}{2}} \frac{e^{-\tau_1}}{\left((2 + e^{-\tau})^K - (2 - e^{-\tau})^K \right)}, \end{aligned}$$

and find

$$K \approx \frac{\ln \coth \left(\frac{\tau_2 - \tau_1}{4} \right)}{\ln(2 + e^{-\tau}) - \ln(2 - e^{-\tau})} \tag{13}$$

$$\approx e^\tau \ln \coth \left(\frac{\tau_2 - \tau_1}{4} \right). \tag{14}$$

We recover here the fundamental property of metastability: the transient length scales exponentially with the average delay time.²¹ For $\tau_1 \approx \tau_2$,

$$K \propto -e^\tau \ln\left(\frac{\tau_2 - \tau_1}{4}\right),$$

and for large difference in delay lengths $\tau_2 - \tau_1 \gg 1$ we find

$$K \propto e^{-\tau_1}.$$

This dependency on the heterogeneity $\tau_2 - \tau_1$ is exemplified in Fig. 8.

A typical time series of these unstable synchronous oscillations in a toggle switch is shown in Fig. 7, together with a phase diagram that shows the diverging oscillators. We indicated the first extrema $\pm 1 \mp a_{1,2}$, $\pm 1 \mp b_{1,2}$, and the corresponding switching times in the graph.

Comparing numerical simulations of the map a_k (Eq. (11)) with the analytic approximation (Eq. (14)), we find that the integer part of the approximation is equal to the numerically obtained number of oscillations in all cases. The numerical results and the approximation are hence indistinguishable in Fig. 8.

C. Generalization to N nodes

This model may be generalized to a ring with N inverters. If all inverters are initialized equally at one of the steady states $x_i(t < 0) = \pm 1$, we can construct a similar map as for the toggle switch (Eq. (11))

$$a_{k+1}^i = \frac{2 - a_k^{i+1}}{2 - a_k^i} a_k^i \quad (15)$$

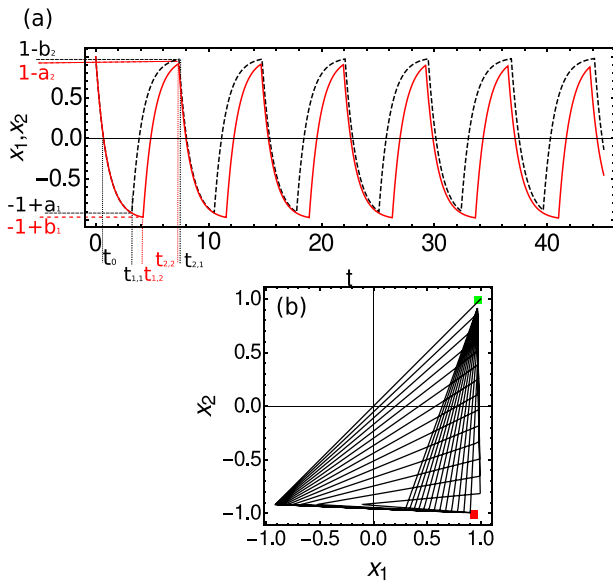


FIG. 7. (a) Time series of $x_1(t)$ (black dashed curve) and $x_2(t)$ (full red curve) in a toggle switch as modeled in Eq. (4). Parameters are $\tau_1 = 2.5$, $\tau_2 = 3.5$ and $m=0$; initial conditions are $x_1(t < 0) = x_2(t < 0) = 1$. The first two switching times and extrema, on which the description as a map is based, are also marked; variables in black (red) relate to the first (second) inverter. (b) Phase diagram of the same time series. The green square indicates the initial conditions (1, 1) and the red square denotes the steady state (1, -1) eventually reached by the toggle switch.

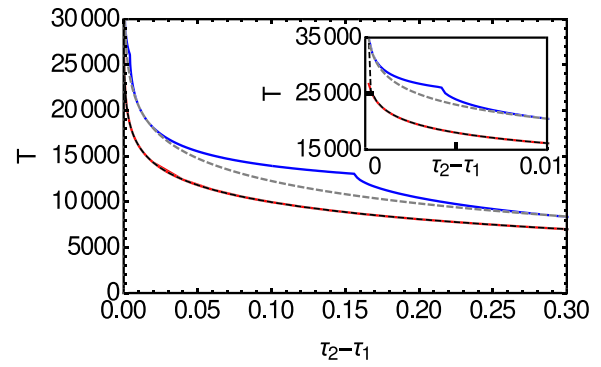


FIG. 8. Duration T of the transient synchronous waves for varying heterogeneity in interaction delays $\tau_2 - \tau_1$, in a toggle switch, obtained by simulating the map (Eq. (11)) (red full line) and by the long delay approximation Eq. (14). The upper blue full curve shows the transient length for a repressilator with similar parameters, obtained by simulating Eq. (15), and the gray dashed curve is the analytically obtained lower bound (Eq. (18)). Parameters are $\tau = 6$, $\delta = 0$ and, for the repressilator $\tau_3 = 6$. The inset zooms in on the transient length for very small heterogeneities between the delays.

with a_k^i the distance of the i -th plateau from the steady states, $N + 1 \equiv 1$ and $\prod a_k^i = e^{-\tau_{tot}}$. This map can be written out as

$$a_k^i = e^{-\tau_i} \frac{\sum_{l=0}^N \exp\left(\sum_{m=1}^l \tau_{i+m-1} - l\tau\right) \sum_{s=1}^N e^{is\theta} (2 - e^{-i\theta - \tau})^k}{\sum_{l=0}^N \exp\left(\sum_{m=1}^l \tau_{i+m} - l\tau\right) \sum_{s=1}^N e^{is\theta} (2 - e^{-i\theta - \tau})^k}, \quad (16)$$

where $\theta = 2\pi/N$.

For a repressilator ($N=3$), the duration of the transient length can then be estimated by calculating the smallest K for which any of the $a_k^i > 1$. In this case, two transitions collide so that one pulse becomes too short and is annihilated and only one transition remains per round trip delay (the stable out-of-phase oscillation). It is no longer possible to determine the number of oscillation cycles K analytically, but the transient length may be estimated graphically. For $N=3$, the denominator in Eq. (16) can be rewritten as

$$\alpha A^k + \beta B^k + \beta^* B^{*k},$$

with $A = 2 - e^{-\tau}$, and $B = 2 - e^{i\theta - \tau}$, $\alpha = 1 + e^{\tau_2 - \tau} + e^{\tau_2 + \tau_3 - 2\tau}$, $\beta = 1 + e^{-i\theta} e^{\tau_2 - \tau} + e^{i\theta} e^{\tau_2 + \tau_3 - 2\tau}$, $\theta = 2\pi/3$ and the star denoting complex conjugation. As an approximation for transient collapse, the denominator equals zero for $k=K$. This leads to a condition

$$\alpha A^K = -2|\beta||B|^K \cos(K\phi + \eta) \iff K = \frac{\ln \alpha - \ln|2\beta| - \ln(-\cos(K\phi + \eta))}{\ln|B| - \ln A}, \quad (17)$$

where $\phi = \arg(B)$ and $\eta = \arg(\beta)$. When $\cos(K\phi + \eta) > 0$, the transient cannot collapse. This phase effect leads to characteristic cusps when calculating the transient lengths for varying heterogeneities. Moreover, we obtain a lower limit for the transient length and recover the exponential scaling of the transient length with the mean time delay

$$K \geq \frac{\ln \alpha - \ln |2\beta|}{\ln |\beta| - \ln A} \geq \frac{4}{3} e^{\tau} \ln \left(\frac{\alpha}{2|\beta|} \right). \quad (18)$$

Figure 8 compares the duration of the in-phase oscillatory transient in the repressilator (obtained by simulations of the map Eq. (15)) and toggle switch, for varying heterogeneity. Although the transients last somewhat longer in the repressilator, the transient duration is of a similar magnitude in both motifs. Cusps in the repressilator transient duration are visible at $\tau_2 - \tau_1 \approx 0.004$ and $\tau_2 - \tau_1 \approx 0.15$.

D. Influence of threshold asymmetries

To better approximate the experiment, we implement asymmetries within each inverter between the rising and falling edge. These asymmetries in the model account for the accumulated effect over the whole delay line. The easiest way to incorporate those in the model is by shifting the threshold of the gate input. The toggle switch is then modeled as

$$\begin{aligned} \dot{x}_1 &= -x_1 + F_1(x_2(t - \tau_1)) \\ \dot{x}_2 &= -x_2 + F_2(x_1(t - \tau_2)), \end{aligned} \quad (19)$$

with

$$F_{1,2}(x) = \begin{cases} 1 & \text{if } x < \delta_{1,2} \\ -1 & \text{if } x \geq \delta_{1,2}. \end{cases} \quad (20)$$

The asymmetry of the gate causes a constant bias: if $\delta > 0$ ($\delta < 0$) a falling (rising) edge is advanced, while a rising (falling) edge experiences a longer delay time. As one edge is always rising in the same gate, and falling in the other, the two edges consistently experience a different bias over the duration of the transient if the gates are nonidentical. In the following, we choose $\delta = \delta_1 = -\delta_2$, but the general case ($\delta_1 \neq \delta_2$) is similar. The effect is not caused by the threshold asymmetries themselves, but by the fact that these are not the same for all inverters in the model, or for all the logical gates in the experiment. In the asymmetric case, for initial conditions $x_i(t \leq 0) = \pm 1$ the map (Eq. (11)) becomes

$$\begin{aligned} a_{k+1} &= a_k \frac{1 + \delta_2 - b_k}{1 - \delta_2 - a_k} \\ b_{k+1} &= b_k \frac{1 - \delta_2 - a_k}{1 + \delta_2 - b_k}, \end{aligned} \quad (21)$$

with $a_k b_k = (1 - \delta^2) e^{-(\tau_1 + \tau_2)}$. The unstable fixed point of the map, which corresponds to synchronous oscillations of the toggle switch, is given by

$$\frac{\delta + 1}{\delta - 1} = \frac{2 - a_1}{2 - b_1}$$

or

$$2\delta \approx e^{-\tau} \sinh \left(\frac{\tau_2 - \tau_1}{2} \right).$$

The map is no longer exactly solvable, but the transient duration may be determined numerically. In Fig. 9(a), we show the transient duration as a function of asymmetry, for different heterogeneities in the delay times. Heterogeneity in the

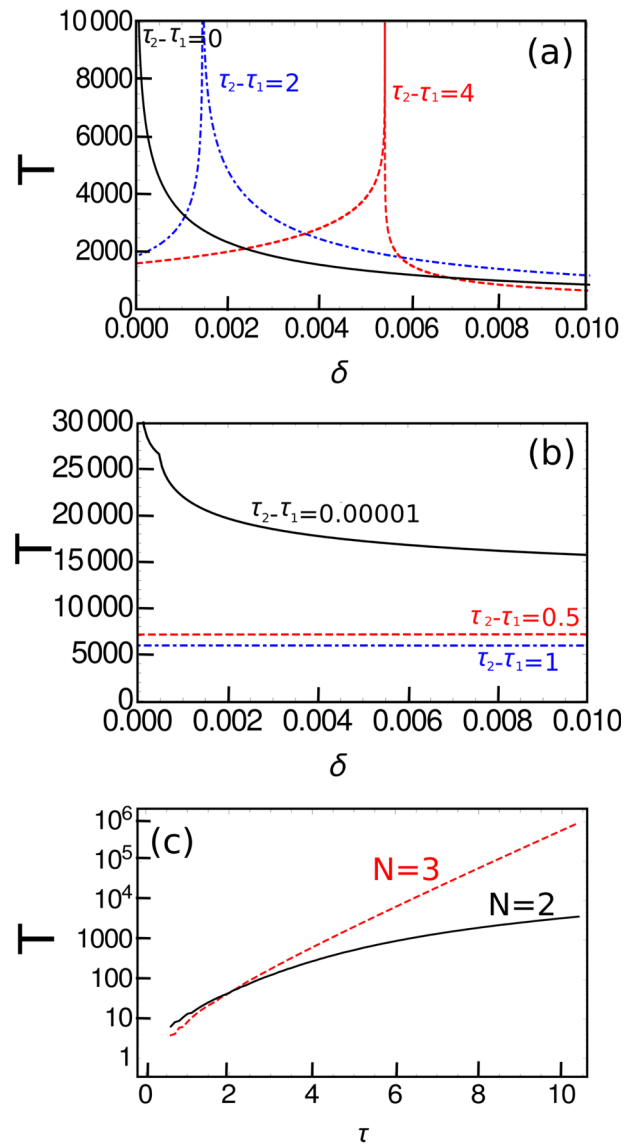


FIG. 9. (a) and (b) Duration T of the transient synchronous oscillations for varying asymmetry δ , in a toggle switch (a) and a repressilator (b). Parameters for the toggle switch are (full black curve) $\tau_i = \tau = 6$, (blue, dashed-dotted) $\tau_1 = 5$, $\tau_2 = 7$ and (red) $\tau_1 = 4$, $\tau_2 = 8$. For the repressilator we chose (full black curve) $\tau_1 = 5.9999$, $\tau_2 = 6.0001$ and $\tau_3 = 6$ (red, dotted) $\tau_1 = 5.75$, $\tau_2 = 6.25$ and $\tau_3 = 6$ and (blue, dashed-dotted) $\tau_1 = 5.5$, $\tau_2 = 6.5$ and $\tau_3 = 6$. (c) Duration of the transient oscillations in a setup with asymmetry, for increasing delay time τ . The red dashed curve shows the repressilator transient length, the full black curve represents the toggle switch. Parameters are $\delta_1 = -\delta_2 = 0.01$ and for the repressilator, $\delta_3 = 0$. The heterogeneity is chosen $\tau_2 - \tau_1 = 0.1$, $\tau_3 = \tau$ (repressilator).

link delays and threshold asymmetry between the gates may compensate each other, and this phenomenon could explain the non-monotonic increase of the transient duration with the link delay in the experiment.

In Fig. 9(c), we show the transient duration for increasing link delays in the presence of a threshold asymmetry. The exponential scaling with the delay can break down for large delay times: When $\delta \gg e^{-\tau}$ holds, the transient length only scales quadratic with the delay, as can be inferred from the map Eq. (21).

For the repressilator (or, more generally, any ring with an odd number of inverters), the threshold asymmetries play

a less important role.²⁰ Rising edges become falling edges (and *vice-versa*) after a round trip, compensating for the effect of threshold asymmetries. Specifically, the general map now reads

$$a_{k+1}^i = \frac{1 + (-1)^{k+1} \delta_j}{1 + (-1)^k \delta_{j+1}} \frac{2 - a_k^{i+1}}{2 - a_k^i} a_n^i. \quad (22)$$

and $j = k \bmod N$.

We show the effect of asymmetry on transient times for the repressilator in Fig. 9(b). The effect is much less pronounced in the repressilator than in the toggle switch. Moreover, we observe similar cusps in the transient length for varying heterogeneity as for varying asymmetry. In Fig. 9(c), where we show the transient length for increasing delay times, in the presence of an asymmetry, the different effect of an asymmetry on the toggle switch and repressilator is even better exemplified, as in the repressilator the transient still increases exponentially with the delay when introducing an asymmetry.

It is interesting to compare our results for the toggle switch with the transient oscillations in a larger ring of an even number of inverters, coupled without delay, as studied by Horikawa and H. Kitajima.^{30,31} We recover the same scaling limit situations for the transient time (Eq. (14)), where the role of the round trip delay in our system is played by the number of inverters in the ring. Also the effect of asymmetries is similar in both models. Our modeling simplification—replacing the inverters in the delay line by a coupling delay, rather than explicitly including their dynamics—thus proves useful.

E. Stochastic delays

In Subsections III A–D, we have only considered deterministic dynamics. However, in the experiments, we observe broad distributions of transients, which cannot be explained based on deterministic dynamics solely, and must result from the small changes as we run the experiment: There are thermal fluctuations in the charge on each gate on a short time scale, and the core temperature and voltage fluctuates on a longer time scale comparable to or shorter than the observed transient times. These effects cause jitter in the delay times of logic elements on the order of 10 ps. Consequently, the experimental delays are inherently stochastic, with variations on the order of 1% of the average time delay.

The description of the system as a map provides a framework to incorporate stochastically varying time delays in a straightforward way. The map describing the toggle switch (Eq. (21)) is adapted in the following way:

$$\begin{aligned} a_{k+1} &= \frac{1 + \delta}{1 - \delta} (2 - b_k) e^{-\Delta t_{1,k}} \\ b_{k+1} &= \frac{1 - \delta}{1 + \delta} (2 - a_k) e^{-\Delta t_{2,k}} \end{aligned} \quad (23)$$

$$\begin{aligned} \Delta t_{1,k+1} &= \Delta t_{1,k} + \ln(2 - a_{k+1}) - \ln(2 - b_k) + \zeta_{1,k+1} - \zeta_{2,k} \\ \Delta t_{2,k+1} &= \Delta t_{2,k} + \ln(2 - b_{k+1}) - \ln(2 - a_k) + \zeta_{2,k+1} - \zeta_{1,k}, \end{aligned}$$

where $\zeta_{j,k}$ denotes white Gaussian noise in the delay times, with zero mean and a variance of σ^2 . Noise in the time delays is implemented in the different Δt_j , which represent the plateau lengths between the consecutive transitions. Without noise, we recover the maps Eqs. (11) and (21). The initial conditions are $a_0 = e^{-\tau_1}$, $b_0 = e^{-\tau_2}$, $\Delta t_{i,0} = \tau_i + \zeta_{i,0} + \ln(2 - e^{-\tau_i})$.

We simulated 10^6 – 10^8 transients in a noisy toggle switch. When considering the most symmetric situation, where heterogeneities and asymmetries are absent ($\tau_1 = \tau_2 = \tau$ and $\delta = 0$, respectively), we observe distributions starting from a minimal length and with an exponential tail. Some typical examples are shown in Fig. 10. The exponential tail decreases slower with the delay time and does not depend on the noise strength. As the noise decreases, however, the minimal transient length increases, and the cutoff becomes less sharp. Overall, as noise and delay grow smaller, the distribution becomes shorter-tailed, similar to our experimental observations for short delays, shown in Fig. 4(a).

We show the scaling of the mean duration time in Fig. 11(a). For small delays and weak noise, we recover the deterministic exponential scaling of the mean transient length with the delay time, as predicted in Eq. (14). In contrast, for stronger noise and larger delays, the mean transient duration scales as a power law with delay time, as shown in the inset. The mean transient duration for varying noise strength is shown in Fig. 11(b): It scales approximately inversely with the noise variance for all delays.

We observe a combination of two effects in the toggle switch model. Without noise, the system drifts slowly towards one of the steady states due to its finite response time. With noise but no internal response time, the system performs a random walk between two absorbing boundaries ($\Delta t_1 = 0$ and $\Delta t_2 = 0$). We see exponential scaling in the mean transient lengths for small noise and short time delays, when the dynamical terms dominate and $e^{-2\tau} > \sigma^2$. As the delay and noise increase, $\sigma^2 > e^{-2\tau}$, and the stochastic terms dominate the dynamics, causing a stochastic power law scaling. Also the shape of the distributions is similar to those

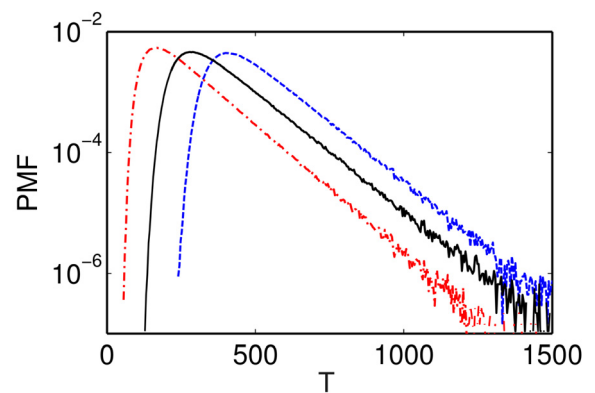


FIG. 10. Probability mass functions (PMF) of the transient lengths T in symmetric noisy toggle switch, for $\tau_1 = \tau_2 = 3.32$, $\delta = 0$ and $\sigma^2 = 0.0001$ (right blue dashed curve), $\sigma^2 = 0.0025$ (middle black full curve) and $\sigma^2 = 0.0081$ (left red dashed-dotted curve). As the noise decreases, the curve resembles more a Gaussian shape (parabolic in a logarithmic plot). The decay of the exponential tail is the same in all three cases however.

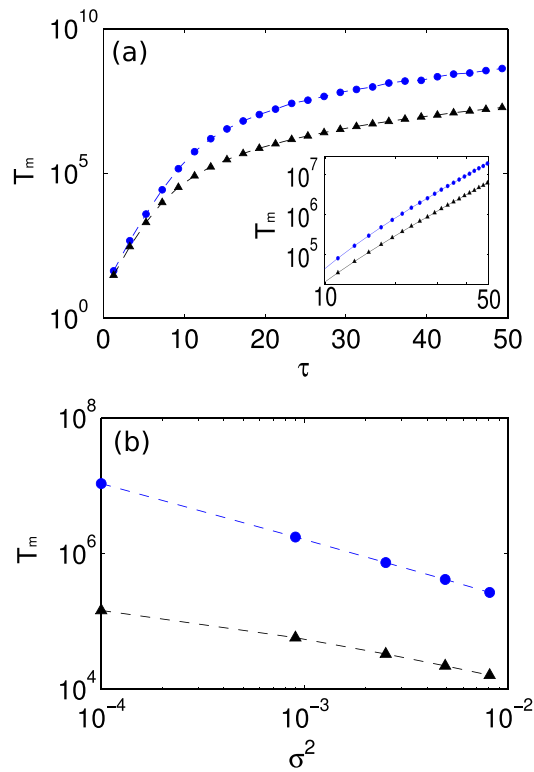


FIG. 11. (a) Mean duration T_m of the transient synchronous waves in a toggle switch for varying mean delay (upper), with symmetric delay lengths $\tau_1 = \tau_2 = \tau$. Noise strengths are $\sigma^2 = 0.0001$ (upper blue circles) and $\sigma^2 = 0.0025$ (lower black triangles). The inset shows the mean transient length for varying delay times in a double logarithmic plot, illustrating the evolution towards polynomial scaling as the delay and noise strength increase. Parameters are $\sigma^2 = 0.0025$ (upper blue circles) and $\sigma^2 = 0.0081$ (lower black triangles). (b) Mean duration of the transient for varying noise strength, for a delay $\tau = 9.31$ (upper blue circles) and $\tau = 19.31$ (lower black triangles).

observed for a symmetric random walk with two absorbing boundaries.³²

The exponential tail of the distribution results from the symmetry of the system. We performed simulations for a gradually increasing asymmetry δ , and some resulting probability density functions are shown in Fig. 12. As the

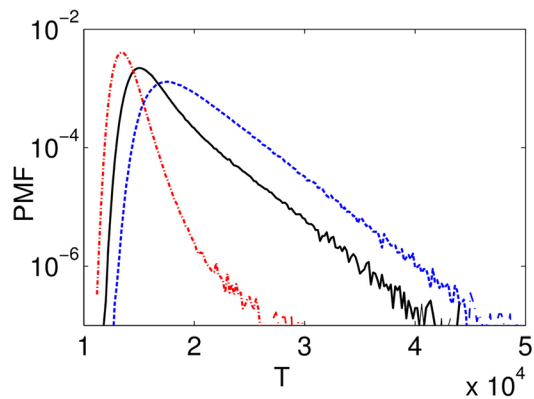


FIG. 12. Probability mass function of the length T of the transient synchronous oscillations in a toggle switch for different asymmetries. The distribution gradually deviates from an exponential as the asymmetry increases. Parameters are $\tau_1 = \tau_2 = 8$, $\sigma^2 = 10^{-8}$ and $\delta = 0$ (right blue dashed curve), $\delta = 0.005$ (middle black full curve), and $\delta = 0.01$ (left red dotted-dashed curve).

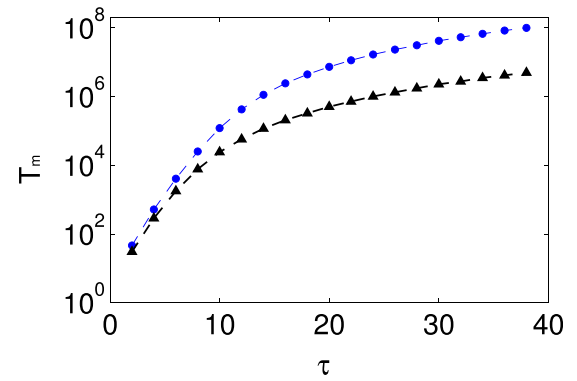


FIG. 13. Mean duration T_m of the transient synchronous oscillations in a repressilator for varying mean delay, with symmetric delay lengths $\tau_1 = \tau_2 = \tau_3 = \tau$. Other parameters are $\sigma^2 = 0.0001$ (upper blue dots) and $\sigma^2 = 0.0025$ (lower black triangles).

asymmetry δ increases, the tail of the distribution gradually changes from exponential into power law as the asymmetry overcomes the noise strength. We thus relate the experimentally measured power law distributions for the toggle switch (Fig. 4) to the asymmetry between rise and fall times in the system.

The results for a symmetric repressilator are similar as for a symmetric toggle switch. We show the mean transient length for varying delays in Fig. 13. Just like for the toggle switch, we observe a transition from exponential scaling to power law scaling with the delay. The distributions have an exponential tail as well, similar to the experimental distributions (shown in Fig. 6).

IV. DISCUSSION

Our experiments show that link delays in ABNs can give rise to extremely long transients in small network motifs. In the toggle switch, we observe these super-transients, with a duration of millions of oscillation cycles or more, for link delays starting from five times the internal response time. These transient patterns appear inconsistently, however, due to sensitivity to logic element heterogeneities and asymmetries. We observe even longer mean transients in the repressilator. Moreover, in this case, the super-transients appear consistently for all experimental setups for long enough link delays.

We reproduce our experimental results in a qualitative way with a simple piecewise linear model with stochastic time delays. Because of the piecewise exponential dynamics and the simple ring structure, we are able to determine analytically the duration of the transient, and retrieve the expected exponential scaling with the delay time. By including stochastic delays in our model, we reproduce the broad distributions that we observe in the experiment. We show how noise can suppress the exponential scaling with the time delay and how the asymmetry can change the shape of the distribution in the toggle switch.

The large number of logic elements on the FPGA enables easy scalability from network motifs to larger

networks with complex topologies. Also our hybrid model involving stochastic link delays can be easily be extended to different Boolean logic and more complex network configurations.

Our experiments suggest that supertransients generally arise in ABNs, if link delays are taken into account. The Boolean approximation of a sigmoidal function in general holds well,¹¹ and thus we conjecture that similar transients occur in networks with switchlike interactions. Moreover, the same transient patterns, however of shorter duration, are observed in more biologically realistic simulations of a toggle switch and repressilator when accounting for the explicit delays arising from transcription and translation processes.¹⁷ Even if in a biologically more realistic context, transients might be a lot shorter-lived in small motifs (in terms of number of oscillations) than in our experimental setup, link delays could still give rise to supertransients in a complex regulatory network. For the functionality of a network, the transient dynamics might hence be relevant as well, and not only the stable attractors.

Our results relate to universal nonlinear phenomena, and are relevant beyond a context of ABNs, or time delay networks. In spatially extended systems, it is well known that the interaction between fronts depends exponentially on their spatial separation.³³ Also transient lengths that increase exponentially with system size have been found in bistable reaction-diffusion systems.³⁴ As a time-delay system can be mapped onto a spatially extended system,³⁵ it makes sense to compare the transitions in our network in terms of fronts.^{36,37} We find a similar scaling, where the smaller plateau length plays the role of the separation between fronts. Moreover, super-transients have been found as well in networks, where the duration scales with number of nodes^{30,38,39} and the phenomenon is related to more complex dynamics, such as transient chaos in coupled maps or spatially extended systems.^{22,23,40–42}

ACKNOWLEDGMENTS

O.D., N.D.H., and D.J.G. gratefully acknowledge the support of U.S. Army Research Office Grant No. W911NF-12-1-0099. J.L. thanks the DFG for support in the framework of SFB 910. We are grateful to Eckehard Schöll and Leon Glass for fruitful discussions.

¹L. Glass and S. Kauffman, "The logical analysis of continuous non-linear biochemical control networks," *J. Theor. Biol.* **39**, 103–129 (1973).

²L. Glass and C. Hill, "Ordered and disordered dynamics in random networks," *Europhys. Lett.* **41**, 599 (1998).

³T. Mestl, C. Lemay, and L. Glass, "Chaos in high-dimensional neural and gene networks," *Physica D* **98**, 33–52 (1996).

⁴H. De Jong, J. Gouze, C. Hernandez, M. Page, T. Sari, and J. Geiselmann, "Qualitative simulation of genetic regulatory networks using piecewise-linear models," *Bull. Math. Biol.* **66**, 301–340 (2004).

⁵R. Edwards and L. Glass, "A calculus for relating the dynamics and structure of complex biological networks," in *Adventures in Chemical Physics: A Special Volume of Advances in Chemical Physics* (Wiley, 2005), Vol. 132, pp. 151–178.

⁶M. Sun, X. Cheng, and J. E. S. Socolar, "Causal structure of oscillations in gene regulatory networks: Boolean analysis of ordinary differential equation attractors," *Chaos* **23**, 025104 (2013).

⁷S. A. Kauffman, "Metabolic stability and epigenesis in randomly constructed genetic nets," *J. Theor. Biol.* **22**, 437–467 (1969).

⁸S. Huang and D. E. Ingber, "Shape-dependent control of cell growth, differentiation, and apoptosis: Switching between attractors in cell regulatory networks," *Exp. Cell Res.* **261**, 91–103 (2000).

⁹S. A. Kauffman and E. D. Weinberger, "The NK model of rugged fitness landscapes and its application to maturation of the immune response," *J. Theor. Biol.* **141**, 211–245 (1989).

¹⁰T. J. Perkins, R. Wilds, and L. Glass, "Robust dynamics in minimal hybrid models of genetic networks," *Phil. Trans. R. Soc. A* **368**, 4961–4975 (2010).

¹¹P. Sharear, L. Glass, R. Wilds, and R. Edwards, "Dynamics in piecewise linear and continuous models of complex switching networks," *Math. Comput. Simul.* **110**, 33–39 (2015).

¹²R. Edwards, A. Machina, G. McGregor, and P. van den Driessche, "A Modelling Framework for Gene Regulatory Networks Including Transcription and Translation," *Bull. Math. Biol.* **77**, 953–983 (2015).

¹³G. Karlebach and R. Shamir, "Modelling and analysis of gene regulatory networks," *Nat. Rev.* **9**, 770 (2008).

¹⁴J. Stricker, S. Cookson, M. R. Bennett, W. H. Mather, L. S. Tsimring, and J. Hasty, "A fast, robust and tunable synthetic gene oscillator," *Nature* **456**, 516 (2008).

¹⁵A. Honkela, J. Peltonen, H. Topa, I. Charapitsa, F. Matarese, K. Grote, H. G. Stunnenberg, G. Reid, N. D. Lawrence, and M. Rattray, "Genome-wide modeling of transcription kinetics reveals patterns of RNA production delays," *Proc. Natl. Acad. Sci.* **112**, 13115–13120 (2015).

¹⁶R. Edwards, P. van den Driessche, and L. Wang, "Periodicity in piecewise-linear switching networks with delay," *J. Math. Biol.* **55**, 271–298 (2007).

¹⁷R. Zhu, A. Ribeiro, D. Salahub, and S. Kauffman, "Studying genetic regulatory networks at the molecular level: Delayed reaction stochastic models," *J. Theor. Biol.* **246**, 725–745 (2007).

¹⁸D. Bratsun, D. Volfson, L. S. Tsimring, and J. Hasty, "Delay-induced stochastic oscillations in gene regulation," *Proc. Natl. Acad. Sci.* **102**, 14593–14598 (2005).

¹⁹T. Erneux, *Applied Delay Differential Equations* (Springer New York, 2009).

²⁰C. Grotta-Ragazzo, K. Pakdaman, and C. Malta, "Metastability for delayed differential equations," *Phys. Rev. E* **60**, 6230 (1999).

²¹K. Pakdaman, C. Grotta-Ragazzo, and C. P. Malta, "Transient regime duration in continuous-time neural networks with delay," *Phys. Rev. E* **58**, 3623–3627 (1998).

²²J. Crutchfield and K. Kaneko, "Are attractors relevant to turbulence," *Phys. Rev. Lett.* **60**, 2715 (1988).

²³T. Tél and Y.-C. Lai, "Chaotic transients in spatially extended systems," *Phys. Rep.* **460**, 245–275 (2008).

²⁴M. B. Elowitz and S. Leibler, "A synthetic oscillatory network of transcriptional regulators," *Nature* **403**, 335 (2000).

²⁵T. S. Gardner, C. R. Cantor, and J. J. Collins, "Construction of a genetic toggle switch in *Escherichia coli*," *Nature* **403**, 339 (2000).

²⁶D. P. Rosin, *Dynamics of Complex Autonomous Boolean Networks* (Springer, Heidelberg, 2015).

²⁷D. P. Rosin, D. Rontani, E. Schöll, and D. J. Gauthier, "Experiments on autonomous Boolean networks," *Chaos* **23**, 025102 (2013).

²⁸H. L. D. d. S. Cavalcante, D. Gauthier, J. E. S. Socolar, and R. Zhang, "On the origin of chaos in autonomous Boolean networks," *Phil. Trans. R. Soc. A* **368**, 495 (2010).

²⁹L. Lücken, J. P. Pade, K. Knauer, and S. Yanchuk, "Reduction of interaction delays in networks," *Europhys. Lett.* **103**, 10006 (2013).

³⁰Y. Horikawa and H. Kitajima, "Duration of transient oscillations in ring networks of unidirectionally coupled neurons," *Physica D* **238**, 216–225 (2009).

³¹Y. Horikawa and H. Kitajima, "Effects of noise and variations on the duration of transient oscillations in unidirectionally coupled bistable ring networks," *Phys. Rev. E* **80**, 021934 (2009).

³²M. Dominé, "First passage time distribution of a Wiener process with drift concerning two elastic barriers," *J. Appl. Prob.* **33**, 164–175 (1996).

³³M. Cross and P. Hohenberg, "Pattern formation outside of equilibrium," *Rev. Mod. Phys.* **65**, 851 (1993).

³⁴Y. Horikawa, "Duration of transient fronts in a bistable reaction-diffusion equation in a one-dimensional bounded domain," *Phys. Rev. E* **78**, 066108 (2008).

- ³⁵G. Giacomelli, R. Meucci, A. Politi, and T. Arrechi, "Defects and space-like properties of delayed dynamical systems," *Phys. Rev. Lett.* **73**, 1099 (1994).
- ³⁶M. Nizette, "Stability of square oscillations in a delayed-feedback system," *Phys. Rev. E* **70**, 056204 (2004).
- ³⁷G. Giacomelli, F. Marino, M. Zaks, and S. Yanchuk, "Coarsening in a bistable system with long-delayed feedback," *Europhys. Lett.* **99**, 58005 (2012).
- ³⁸M. Wolfrum and O. E. Omel'chenko, "Chimera states are chaotic transients," *Phys. Rev. E* **84**, 015201 (2011).
- ³⁹D. P. Rosin, D. Rontani, N. D. Haynes, E. Schöll, and D. J. Gauthier, "Transient scaling and resurgence of chimera states in networks of Boolean phase oscillators," *Phys. Rev. E* **90**, 030902 (2014).
- ⁴⁰A. Wacker, S. Bose, and E. Schöll, "Transient spatiotemporal chaos in a reaction-diffusion model," *Europhys. Lett.* **31**, 257 (1995).
- ⁴¹B. Hof, J. Westerweel, T. M. Schneider, and B. Eckhardt, "Finite lifetime of turbulence in shear flows," *Nature* **443**, 59–62 (2006).
- ⁴²J. Paris and R. Tavakol, "Goodstein algorithm as a super-transient dynamical system," *Phys. Lett. A* **180**, 83–86 (1993).